

3D to 4D Facial Expressions Generation Guided by Landmarks

Naima Otberdout

Univ. Lille, CNRS, Centrale Lille, UMR 9189 CRISTAL, F-59000 Lille, France

naima.otberdout@univ-lille.fr

Claudio Ferrari

Media Integration ad Communication Center

University of Florence, Italy

claudio.ferrari@unifi.it

Mohamed Daoudi

IMT Lille Douai, Institut Mines-Télécom, Univ. Lille, Centre for Digital Systems, F-59000 Lille, France
Univ. Lille, CNRS, Centrale Lille, Institut Mines-Télécom, UMR 9189 CRISTAL, F-59000 Lille, France

mohamed.daoudi@imt-lille-douai.fr

Stefano Berretti

Media Integration ad Communication Center

University of Florence, Italy

stefano.berretti@unifi.it

Alberto Del Bimbo

Media Integration ad Communication Center

University of Florence, Italy

alberto.delbimbo@unifi.it

Abstract

While deep learning-based 3D face generation has made a progress recently, the problem of dynamic 3D (4D) facial expression synthesis is less investigated. In this paper, we propose a novel solution to the following question: given one input 3D neutral face, can we generate dynamic 3D (4D) facial expressions from it? To tackle this problem, we first propose a mesh encoder-decoder architecture (Expr-ED) that exploits a set of 3D landmarks to generate an expressive 3D face from its neutral counterpart. Then, we extend it to 4D by modeling the temporal dynamics of facial expressions using a manifold-valued GAN capable of generating a sequence of 3D landmarks from an expression label (Motion3DGAN). The generated landmarks are fed into the mesh encoder-decoder, ultimately producing a sequence of 3D expressive faces. By decoupling the two steps, we separately address the non-linearity induced by the mesh deformation and motion dynamics. The experimental results on the CoMA dataset show that our mesh encoder-decoder guided by landmarks brings a significant improvement with respect to other landmark-based 3D fitting approaches, and that we can generate high quality dynamic facial expressions. This framework further enables the 3D expression intensity to be continuously adapted from low to high intensity. Finally, we show our framework can be applied to

other tasks, such as 2D-3D facial expression transfer.

1. Introduction

Facial animation aims at generating realistic face instances that dynamically evolve across time showing varying expressions or speech-related movements. It finds application in a wide range of graphics contexts spanning from 3D face modeling, to augmented and virtual reality for animated films and computer games. In Computer Graphics various techniques have been proposed to capture the facial expression of a subject and transfer it to a target model [8]. In these solutions, a real tracked facial movement is transferred to an avatar. Instead, here we are interested in animating a face just starting from a neutral face and some additional attributes, like an expression label or a speech track. In this scenario, retaining the identity of the input subject in the generated instances is a natural requirement. Recent advances in generative neural networks have made possible effective solutions that operate on 2D images [14, 26]. These solutions try to decouple the temporal and the appearance generation or generate them together; another distinctive aspect is given by the input attributes that condition the frame generation from the given image. Examples include a vector of numbers indicating the intensity of the generated

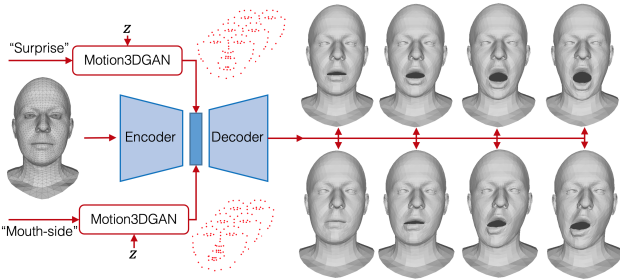


Figure 1. Overview of our method. The Expr-ED network generates an expressive 3D face from its neutral counterpart given a set of target landmarks. The Motion3DGAN generates a sequence of 3D landmarks from noise and an expression label. The sequence of landmarks is fed to Expr-ED to generate a 4D facial expression.

expression frame-by-frame [14, 34], or the initial configuration of facial landmarks [26].

In contrast, few studies have addressed the problem of facial animation in 3D. Some works tried to animate a 3D face mesh given an arbitrary speech signal and a static 3D face mesh as input [10, 20]. Such speech-driven facial animation approaches do not account for facial expressions, which are instead a major component to convey emotion in the entertainment industry. To the best of our knowledge, the work in [28] is the only one that can generate a dynamic sequence of expressive 3D meshes given a reference neutral mesh, together with an expression label of the sequence and a per frame intensity value.

In this work, we propose a solution for 3D face animation that only requires a 3D neutral face mesh and the expression label of the target sequence as inputs, and generates a dynamic sequence of 3D meshes with the given expression. The approach, illustrated in Figure 1, develops on the idea of using landmarks of the face to model the temporal behavior of the face across time, while separating this behavior from the reconstruction of the shape. This is obtained with a two-step solution: (i) In the first step, a *conditional manifold-valued Wasserstein GAN* (Motion3DGAN) generates the 3D configuration of facial landmarks across time starting from noise and an expression label. The manifold-valued GAN has the advantage of generating the overall temporal dynamics as a point on the unit hypersphere, which makes the generated sequence smooth and controllable. (ii) Then, a neutral 3D model and the generated sequence of landmark configurations are the input to an encoder-decoder network (Expr-ED). The encoder learns a latent vector exploiting the *spiral convolution* operation [5] on the mesh, and the vertex proximity to the landmarks. The decoder reconstructs the mesh for each frame of the sequence starting from the latent representation concatenated with the landmarks configuration of that frame. Experiments conducted on the CoMA dataset [29], show the proposed method can generate realistic sequences

of 3D expressive face models, with a reconstruction error much lower than PCA. We also verified the generated expressions are classified with an accuracy which is superior to that of compared solutions. Finally, we also show that realistic 3D reconstructions can be derived from landmarks extracted from a 2D image and a generic 3D template.

The main contributions of our work are: (i) we propose an original method to generate dynamic sequences of 3D expressive scans given a neutral 3D mesh and an expression label. Our approach has the capability of generating strong and asymmetric expressions; (ii) we adapt a specific GAN architecture for dynamic 3D landmarks generation, and design an encoder-decoder for expressive mesh reconstruction from a neutral mesh and landmarks. Differently from common auto-encoders, the proposed encoder-decoder is the first one capable of reconstructing expressive meshes from neutral ones; (iii) the proposed Expr-ED generalizes well to unseen expressions not present in the training, making it possible to extend its use to other expression classes.

2. Related Work

Our work is related to methods for facial expression generation guided by landmarks, 3D face generation, and dynamic generation of 3D faces, *i.e.*, 4D face generation.

Facial expression generation guided by landmarks. Thanks to the recent advances in neural network computation, landmark detection from human faces is now reliable and accurate [9, 12, 24, 32]. Landmarks are a viable way to account for facial deformation and considering only their motion reduces the complexity of the visual data. Based on these considerations, some recent works developed on the idea of generating sequences of landmark configurations. Wang *et al.* [33] proposed a framework that decouples information about facial expression dynamics, encoded into landmarks, and face appearance. This was obtained by a conditional recurrent network, where the first layer generates a sequence of facial landmark embedding, conditioned on a given facial expression label and an initial configuration of face landmarks. Otberdout *et al.* [26] proposed an approach for generating videos of the six basic facial expressions given a neutral face image. The face geometry is captured by modeling the motion of facial landmarks as curves encoded as points on a hypersphere. A manifold-valued GAN learns the distribution of expression dynamics.

These methods generate the motion of 2D landmarks, while our work is the first one to tackle the problem of modeling the 3D facial motion by generating the temporal dynamics of 3D landmarks.

3D face generation. The 3D Morphable Model (3DMM) as originally proposed in [3] and its variants [4, 15, 27] have been widely used in several face applications. They are based on a linear formulation, so non-linear encoder-decoder architectures are now attracting more and

more attention for reconstructing 3D face with improved representation capabilities. This comes at the cost of reformulating convolution and pooling/unpooling like operations on the non-regular mesh support [6, 23, 31]. Ranjan *et al.* [29] proposed an auto-encoder architecture that learns a non-linear representation of a 3D face mesh. To this end they defined a spectral convolution operation on the mesh and also a pooling operation to down-/up-sample the mesh. Bouritsas *et al.* [5] proposed a novel graph convolutional operator, acting directly on the 3D mesh. This enforces consistent local orderings of the vertices of the graph through the *spiral operator* [22]. Abrevaya *et al.* [1] proposed a framework that learns a generative 3D face model using an auto-encoder architecture that combines a CNN-based encoder with a multi-linear model-based decoder. However, this approach first projects the input 3D scan to a depth image. To retain the high frequency details of 3D faces, a GAN modeling the distribution of 3D facial surfaces was proposed by Moschoglou *et al.* [25]. Also this approach does not operate on the mesh, but on a UV-map.

Differently from the previous literature, we go beyond self-reconstruction and extend the encoder-decoder architecture so to generate an expressive mesh from its neutral counterpart directly in the 3D space. This is achieved using only a set of 3D landmarks as guidance.

4D face generation. While many researches tackled the problem of 3D mesh deformation, the task of 3D facial motion synthesis is yet more challenging. Indeed, a few studies addressed this issue by exploiting audio features to generate facial motions [34, 20]. Potamias *et al.* [28] were the first proposing to generate a facial animation sequence of expressive 3D face models given a neutral 3D model. An LSTM network was used to encode the temporal dynamics starting from an expression label given as a one-hot encoding of one among six expressions along with intensity. A mesh decoder was then used frame-by-frame to reconstruct an expressive mesh from the neutral mesh and the latent code produced by the LSTM.

The approach in [28] is the closest one to our work. As opposed to [28], we propose to guide the 4D facial expression generation using 3D facial landmarks. By doing so, we propose a model with high generalization capability that can generate strong and unseen expressions. We evaluate our model on the CoMA dataset, which contains stronger expressions, more classes and less data than that used in [28] (we could not use the data of [28] as it is not publicly available). However, even using a more challenging dataset, we were able to generate high quality dynamic expressions with smooth motion and controllable intensity. Furthermore, while in [28] an LSTM is used that takes discrete codes with incremental intensity to generate the dynamics, we encode the motion information of the facial expression in one compact representation. This allows us to

generate smoother motions and avoid the error accumulation that is usually encountered with recurrent models. In addition, this compact representation allows us to transfer facial expressions from 2D or 3D faces to another 3D face.

3. Proposed method

Our approach consists of two specialized sub-networks: the first one, Expr-ED, is a mesh encoder-decoder that we train to reconstruct an expressive 3D face given a neutral 3D face and a configuration of 3D landmarks. The second, called Motion3DGAN, generates a sequence of 3D landmarks from noise, provided an expression label, *e.g.*, happy, angry. The landmarks sequence is fed to Expr-ED, which ultimately generates a sequence of expressive 3D faces corresponding to the initial expression label.

3.1. 3D mesh encoder-decoder (Expr-ED)

In the following, we assume all the meshes have a fixed topology and are in full point-to-point correspondence. Let $\mathcal{L} = \{(\mathbf{S}_1^n, \mathbf{S}_1^e, \mathbf{Z}_1^e), \dots, (\mathbf{S}_m^n, \mathbf{S}_m^e, \mathbf{Z}_m^e)\}$ be the training set, where $\mathbf{S}_i^n = (p_1^n, \dots, p_N^n) \in \mathbb{R}^{N \times 3}$ is a neutral 3D face, $\mathbf{S}_i^e = (p_1^e, \dots, p_N^e) \in \mathbb{R}^{N \times 3}$ is a 3D expressive face, and $\mathbf{Z}_i^e \in \mathbb{R}^{n \times 3}$ the 3D landmarks corresponding to \mathbf{S}_i^e .

Our goal here is to find a mapping $h : \mathbb{R}^{N \times 3} \rightarrow \mathbb{R}^{N \times 3}$ such that $\mathbf{S}_i^e \approx h(\mathbf{S}_i^n, \mathbf{Z}_i^e)$. Traditional models learn a latent representation of a 3D face using a linear function h (sub-space) such as PCA. Due to this linearity, they cannot capture extreme deformations and non-linear details. Adapting the idea of the auto-encoder proposed by Ranjan *et al.* [29], we design the function h as an encoder-decoder network (Expr-ED) where the mapping is between a neutral 3D face and a 3D face showing an expression. This is obtained by combining three main operations: (i) a specific mesh convolution operator, *i.e.*, *spiral convolution* with related down-/up-sampling of the mesh; (ii) the concatenation of the latent vector encoding the input mesh with the 3D landmarks of the target expression; (iii) a new loss function that weighs each vertex reconstruction on a landmarks' proximity basis.

Figure 2 summarizes the proposed encoder-decoder architecture. The input to the encoder is a neutral face mesh with the 3D coordinates of $N = 5023$ vertices. The mesh passes through four layers that perform spiral convolution and mesh downsampling. Compared to other mesh convolution operators, like spectral convolution [29] or [17], the spiral convolution is simple to implement and showed its effectiveness in other works [5]. The fully connected layer FC1 encodes the mesh into a 16-dimensional latent space. The latent vector is then concatenated with $n = 68$ landmarks of the face spatially disposed according to the target expression (for concatenation, the 3D landmark coordinates are vectorized to a 204-dimensional vector). The decoder starts with the FC2 layer that brings the linear vector back to $\mathbb{R}^{21 \times 128}$; Four more layers, each performing spiral con-

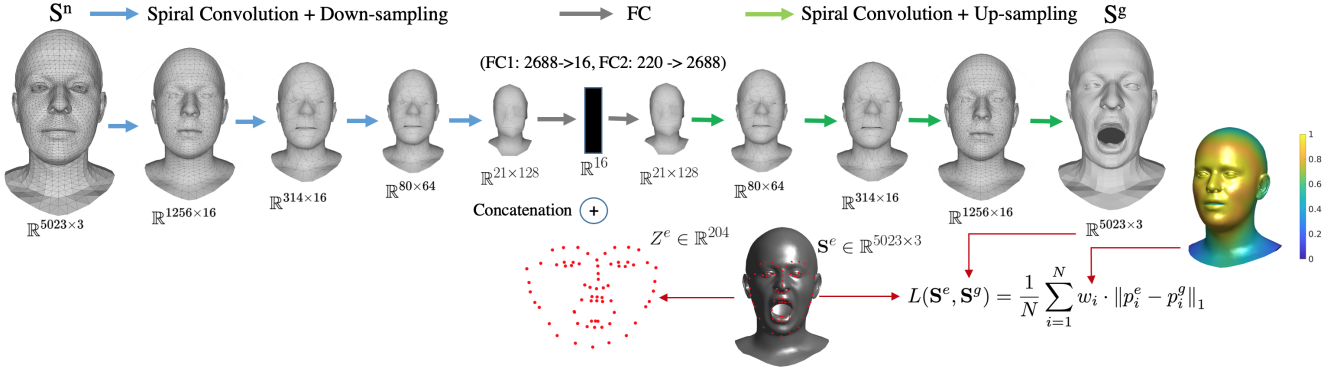


Figure 2. Overview of our method. The encoder maps the neutral face \mathbf{S}^n into a 16-dimensional vector. The 68 target landmarks Z^e are vectorized and concatenated to the latent vector to form a 220-dimensional vector that is decoded to generate the expressive face \mathbf{S}^g . The loss is computed between the ground-truth expressive face \mathbf{S}^e and \mathbf{S}^g . The colored model visualizes the distribution of the weights.

volution plus upsampling, generate the 3D output mesh with an expression which is as close as possible to that shown by the landmarks. The network is trained under the control of the proposed weighted $L1$ loss.

Loss Function. Previous works using encoder-decoder architectures [5, 29], trained the network towards self-reconstruction. Using the notation of Section 3.1, this corresponds to finding a function h such that $\mathbf{S}^g \approx h(\mathbf{S}^{in})$. This is achieved by minimizing the $L1$ loss, computed between the input mesh \mathbf{S}^{in} and the generated output \mathbf{S}^g . Differently, we aim at generating a novel 3D face \mathbf{S}^g reproducing the expression provided by the target landmarks Z^e , yet maintaining the identity structure of \mathbf{S}^n . So, we train the network by minimizing the error between \mathbf{S}^g and \mathbf{S}^e . However, we observed that, in this scenario, some regions of the neutral 3D face need to be deformed to a greater extent in order to reproduce strong expressions. Incidentally, the regions that are subject to stronger motions under facial expressions are those around the landmarks, *e.g.*, mouth, eyes. Other regions like the forehead, instead, remain relatively stable. Our intuition consists in giving more importance to those movable regions, which is achieved by defining a weighted version of the $L1$ loss:

$$L(\mathbf{S}^e, \mathbf{S}^g) = \frac{1}{N} \sum_{i=1}^N w_i \cdot \|p_i^e - p_i^g\|_1. \quad (1)$$

We define the weights as the inverse of the Euclidean distance of each vertex p_i in the mesh from its closest landmark Z_j . This provides a coarse indication of the location of each p_i , and how much it contributes to the expression generation. Given that the mesh topology is fixed, we can pre-compute the weights w_i and re-use them for each sample. For each p_i on the template mesh, we compute the weight as, $w_i = \frac{1}{\min d(p_i, Z_j)}$ $\forall j$, where $d(\cdot)$ is the Euclidean distance. Weights are then re-scaled so that they lie in the $[0, 1]$ range. Vertices corresponding to the landmarks,

i.e., $p_i = Z_j$ for some j , are hence assigned the maximum weight. We will show this simple strategy provides a significant improvement with respect to the standard $L1$ loss.

3.2. Generating 4D expression sequences

Facial landmarks have been proven to well encode the temporal evolution of facial expressions [19, 26]. Motivated by this fact, we generate the facial expression motion based on the motion of 3D facial landmarks. Given a set of n 3D landmarks, $Z(t) = (x_i(t), y_i(t), z_i(t))_{i=1}^n$, their motion can be formulated as a parametrized curve in the 3D space. Let $\alpha : I \rightarrow \mathbb{R}^{n \times 3}$ represents the parametrized curve. For the purpose of modeling and studying our curves, we adopt the square-root velocity function (SRVF) proposed in [30]. For a given curve $\alpha(t) : I \rightarrow \mathbb{R}^{n \times 3}$, the square-root velocity function (SRVF) $q(t) : I \rightarrow \mathbb{R}^{n \times 3}$ is defined by:

$$q(t) = \frac{\dot{\alpha}(t)}{\sqrt{\|\dot{\alpha}(t)\|}}. \quad (2)$$

This function was successfully exploited for human action recognition [11] and 3D face recognition [13]. Otberdout *et al.* [26] proposed to use the SRVF representation to model the temporal evolution of 2D facial landmarks as a point on a hypersphere, which makes it possible to learn the distribution of these points and generate new 2D facial expression motions. In this paper, we extend this idea to 3D by proposing the Motion3DGAN model that we use to generate sequences of 3D facial landmarks. To this end, we represent the motion of 3D facial landmarks by the SRVF representation in (2). This representation is reversible, which makes it possible to easily recover facial landmarks $\alpha(t)$ from a new generated SRVF $q(t)$ by,

$$\alpha(t) = \int_0^t \|q(s)\| q(s) ds + \alpha(0), \quad (3)$$

where $\alpha(0)$ corresponds to the 3D landmark configuration of the neutral face. Using this equation, we can apply

the generated motion to any facial landmark configuration, which we can exploit to perform facial expression transfer.

Following [26], we remove the scale variability of the resulting motions by scaling the \mathbb{L}^2 -norm of these functions to 1 (*i.e.*, $\|q\| = 1$). As a result, we transform the motion of 3D facial landmarks to points on a hypersphere space $\mathcal{C} = \{q : [0, 1] \rightarrow \mathbb{R}^{n \times 3}, \|q\| = 1\}$. The resulting representations are manifold-valued data that cannot be handled with traditional generative models.

In order to learn the distribution of the SRVF representations, we propose Motion3DGAN as an extension of MotionGAN [26], *i.e.*, a conditional version of the Wasserstein GAN for manifold-valued data [18] that resides in a hypersphere \mathcal{C} . It maps a random vector z to a point on the hypersphere \mathcal{C} conditioned on an input class label. Motion3DGAN is composed of two networks trained adversarially, a generator G that aims to learn the distribution of the 3D landmark motions and the discriminator D that distinguishes between real and generated 3D landmark motions. The loss function used to train Motion3DGAN is given by a weighted sum of the adversarial loss L_{adv} and the reconstruction loss L_r such that $L_M = \alpha_1 L_{adv} + \alpha_2 L_r$, where

$$L_{adv} = \mathbb{E}_{q \sim \mathbb{P}_q} [D(\log_p(q), c)] - \mathbb{E}_{z \sim \mathbb{P}_z} [D(\log_p(\exp_p(G(z, c))))] + \lambda \mathbb{E}_{\hat{q} \sim \mathbb{P}_{\hat{q}}} [(\|\nabla_{\hat{q}} D(\hat{q})\|_2 - 1)^2]. \quad (4)$$

In the above equation, c is the expression label (*e.g.*, mouth open, eyebrow) that we encode as a vector concatenated with a random noise $z \sim \mathbb{P}_z$, $q \sim \mathbb{P}_q$ is an SRVF sample from the training set. The last term of the adversarial loss represents the gradient penalty of Wasserstein GAN [16]. Specifically, $\hat{q} \sim \mathbb{P}_{\hat{q}}$ is a random point sampled uniformly along straight lines between pairs of points sampled from \mathbb{P}_q and the generated distribution \mathbb{P}_g . It is given by,

$$\hat{q} = (1 - \tau) \log_p(q) + \tau \log_p(\exp_p(G(z, c))), \quad (5)$$

where $0 \leq \tau \leq 1$ and $\nabla_{\hat{q}} D(\hat{q})$ is the gradient *w.r.t.* \hat{q} . The functions $\log_p(\cdot)$ and $\exp_p(\cdot)$ are the logarithm and the exponential maps, respectively, defined in a particular point p of the hypersphere manifold. They are used to map the SRVF data back and forth to a tangent space of \mathcal{C} ,

$$\begin{aligned} \log_p(q) &= \frac{d_{\mathcal{C}}(q, p)}{\sin(d_{\mathcal{C}}(q, p))} (q - \cos(d_{\mathcal{C}}(q, p))p), \\ \exp_p(s) &= \cos(\|s\|)p + \sin(\|s\|) \frac{s}{\|s\|}, \end{aligned} \quad (6)$$

where $d_{\mathcal{C}}(q, p) = \cos^{-1}(\langle q, p \rangle)$ is the distance between q and p in \mathcal{C} .

The reconstruction loss used to train Motion3DGAN with the adversarial loss is defined by,

$$L_r = \|\log_p(\exp_p(G(z, c))) - \log_p(q)\|_1, \quad (7)$$

where $\|\cdot\|_1$ represents the L_1 -norm and q is the ground truth SRVF corresponding to the condition c .

4. Experiments

4.1. Dataset and experimental setting

In our experiments, we used the CoMA dataset [29], which is a common benchmark employed in other studies [5, 29]. It consists of 12 subjects, each one performing 12 extreme and asymmetric expressions. Each expression comes as a sequence of meshes $\mathbf{S} \in \mathbb{R}^{N \times 3}$, with $N = 5023$ vertices, and an average of 140 meshes per sequence.

For training the Expr-ED network, we used the *extrapolation* protocol as defined in [29], so to verify the generalization to unseen expressions. According to this protocol, we train the model on 11 expressions and test on the leftover expression, performing a 12-fold cross validation. For Motion3DGAN training, we used all CoMA as training set, since we generate from a random noise during test time. We divided each sequence of CoMA into sub-sequences of length 30, starting from the neutral to the apex frame. Then, we encoded the motion of 68 landmarks from the sub-sequences in the SRVF representations, and used them to train Motion3DGAN. Each of the 12 expression labels was encoded as a one-hot vector, concatenated with a random noise vector of size 128. The architectures of the generator and the discriminator are similar to [26].

We trained both Motion3DGAN and Expr-ED using the Adam optimizer, with learning rate of 0.0001 and 0.001 and mini-batches of size 128 and 16, respectively. Motion3DGAN was trained for 600 epochs, while 300 epochs were adopted for Expr-ED. The hyper-parameters of Motion3DGAN loss were set empirically to $\alpha_1 = 1$ and $\alpha_2 = 10$. We chose the mean SRVF of CoMA data as a reference point p , where we defined the tangent space of \mathcal{C} . To compare our generated meshes with other methods, we exploit the mean per-vertex Euclidean error between the generated meshes and their corresponding ground truth.

4.2. Comparison with L_1 loss

We first present an ablation study relative to the proposed weighted L_1 loss. In order to showcase the importance of weighting the contribution of each vertex to the expression generation, we compare the results obtained using our proposed loss against the standard L_1 loss, *i.e.* where $w_i = 1 \forall i$. Figure 3 reports a comparison for each expression, where the remarkable improvement of our proposed loss against L_1 turns out evidently. To better visualize the effect of our loss on the generated meshes, we show two examples in Figure 4. Assigning a greater weight to movable face parts allows the network to focus on those regions that are subject to strong facial motions, ultimately resulting in realistic samples. Without such constraint, the generated

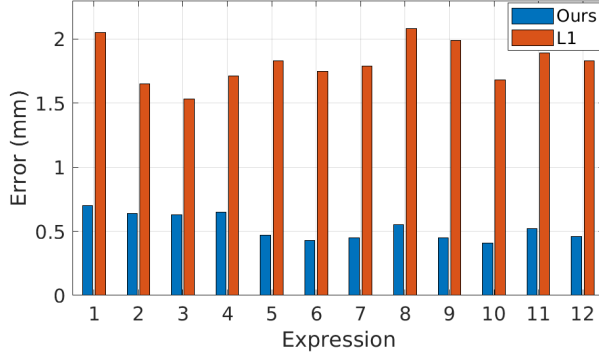


Figure 3. Comparison between our weighted loss and standard L1.

meshes show only some limited deformation.

4.3. Comparison with shape fitting methods

The proposed method generates an expressive mesh \mathbf{S}^g of a subject, given as input its corresponding mesh in neutral expression \mathbf{S}^n and a set of target 3D landmarks $Z^e \in \mathbb{R}^{n \times 3}$ of some expression. We evaluate the accuracy of our approach by comparing against landmark-based deformable model fitting methods. To perform this comparison, we first build a 3DMM transforming the training set of 3D faces into a vector space representation based on PCA [3]. The resulting k principal components $\mathbf{C} = [\mathbf{c}_1, \dots, \mathbf{c}_k] \in \mathbb{R}^{k \times N \times 3}$, with $\mathbf{c}_i \in \mathbb{R}^{N \times 3}$, describe the facial shape variations and are used to generate novel shapes \mathbf{S}^g by deforming an average face shape $\mathbf{m} \in \mathbb{R}^{N \times 3}$. This is achieved by linearly combining the components \mathbf{c}_i :

$$\mathbf{S}^g = \mathbf{m} + \sum_{i=1}^k \mathbf{c}_i \alpha_i. \quad (8)$$

With this framework, arbitrary yet plausible face shapes can be generated by manipulating the deformation coefficients $\alpha \in \mathbb{R}^k$. Similarly to previous works [15, 21], we aim at using this framework to deform the 3D face of an individual in neutral expression \mathbf{S}^n and generate an expressive face shape \mathbf{S}^e of the same individual by fitting \mathbf{S}^n to the set of target landmarks Z^e . To do so, we first need to select a corresponding set of landmarks from \mathbf{S}^n . Given the fixed topology of the 3D faces, we can retrieve the landmark coordinates by indexing into the mesh, *i.e.*, $Z^n = \mathbf{S}^n(\mathbf{I}_z)$, where $\mathbf{I}_z \in \mathbb{N}^n$ are the indices of the vertices that correspond to the landmarks. We then find the optimal deformation coefficients $\hat{\alpha}$ that minimize the Euclidean error between the target landmarks Z^e and the neutral ones Z^n .

To perform the fitting using the 3D landmark pairs, we need to select the corresponding entries from the deformation components \mathbf{c}_i . In fact, each j -th element of the i -th component $\mathbf{c}_{(i,j)}$ controls the deformation of the j -th ver-

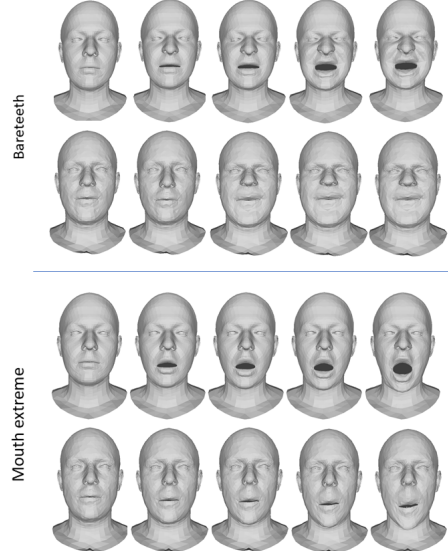


Figure 4. Ablation study: qualitative comparison between our model with (top row) and without (bottom row) weighted loss.

tex in the mesh. So, the problem is formulated as:

$$\hat{\alpha} = \min_{\alpha} \left\| Z^e - Z^n - \sum_{i=1}^k \mathbf{c}_i(\mathbf{I}_z) \alpha_i \right\|_2. \quad (9)$$

By precomputing the distance $\delta_Z = Z^e - Z^n$, the solution to the above linear least squares is found in closed form as $\hat{\alpha} = \mathbf{C}^{-1} \cdot \delta_Z$. Given the optimal coefficients $\hat{\alpha}$, we then generate the expressive shape \mathbf{S}^e by deforming \mathbf{S}^n using (8). The error is computed between the generated mesh \mathbf{S}^g and the ground-truth one \mathbf{S}^e . This provides us an estimate of how faithfully the model can generate an expressive face under the guidance of a set of sparse landmarks.

In the literature, other than PCA several variants have been proposed to learn the components \mathbf{C} . We experimented the standard PCA-based 3DMM, the DL-3DMM [15], and the FLAME model [21]. The DL-3DMM showed improved modeling capabilities by removing the orthogonality constraint imposed by PCA. FLAME instead is a state-of-the-art model for face representation that combines linear blend skinning for head and jaw motion with linear PCA spaces to represent identity and expression shape variations. For PCA, we employed different numbers of principal components, that is 16, 38 and 220. The first corresponds to the size of the latent vector as resulting from encoding \mathbf{S}^n ; the second corresponds to the number required to retain the 99% of the variance (as standard practice); the last one corresponds to the size of the input to the decoder, *i.e.*, 16 plus the vectorized landmarks. For the DL-3DMM, we chose to use 220 dictionary atoms as using fewer did not provide significant results. For FLAME, we

Expression	PCA-16	PCA-38	PCA-220	DL [15]-220	Flame [21]	Ours
Bareteeth	1.72 \pm 1.09	1.10 \pm 0.66	1.10 \pm 0.67	1.11 \pm 0.63	6.95 \pm 4.07	0.70 \pm 0.93
Cheeks-in	1.60 \pm 1.02	1.12 \pm 0.72	1.01 \pm 0.72	1.17 \pm 0.80	5.49 \pm 3.63	0.64 \pm 0.84
Eyebrow	0.94 \pm 0.73	0.77 \pm 0.57	1.17 \pm 0.95	1.13 \pm 0.75	5.76 \pm 3.74	0.63 \pm 0.94
High Smile	1.53 \pm 1.02	1.02 \pm 0.66	0.93 \pm 0.55	1.05 \pm 0.62	6.70 \pm 4.26	0.65 \pm 0.96
Lips Back	1.71 \pm 1.11	1.04 \pm 0.62	0.89 \pm 0.50	1.02 \pm 0.57	6.15 \pm 4.29	0.47 \pm 0.58
Lips up	1.17 \pm 0.69	0.84 \pm 0.52	0.88 \pm 0.51	0.98 \pm 0.56	6.08 \pm 4.49	0.43 \pm 0.47
Mouth down	1.29 \pm 0.86	0.86 \pm 0.54	0.78 \pm 0.43	0.87 \pm 0.48	5.83 \pm 3.86	0.45 \pm 0.57
Mouth Extreme	1.54 \pm 1.20	1.05 \pm 0.70	0.92 \pm 0.55	0.99 \pm 0.58	6.67 \pm 5.98	0.55 \pm 0.7
Mouth middle	1.37 \pm 0.87	0.87 \pm 0.53	0.75 \pm 0.42	0.85 \pm 0.47	5.95 \pm 3.90	0.45 \pm 0.52
Mouth Open	1.14 \pm 0.86	0.78 \pm 0.54	0.73 \pm 0.45	0.82 \pm 0.51	5.68 \pm 4.71	0.41 \pm 0.49
Mouth side	1.35 \pm 0.92	1.21 \pm 0.82	1.00 \pm 0.64	1.14 \pm 0.72	6.31 \pm 4.80	0.52 \pm 0.67
Mouth up	1.31 \pm 0.88	0.94 \pm 0.61	0.87 \pm 0.53	0.94 \pm 0.56	5.98 \pm 3.88	0.46 \pm 0.56
Total	1.38 \pm 0.87	0.97 \pm 0.62	0.91 \pm 0.57	1.01 \pm 0.61	6.12 \pm 4.29	0.53 \pm 0.68

Table 1. Reconstruction error (mm): comparison with PCA- k (k principal components), the DL-3DMM (220 dictionary atoms), and Flame.

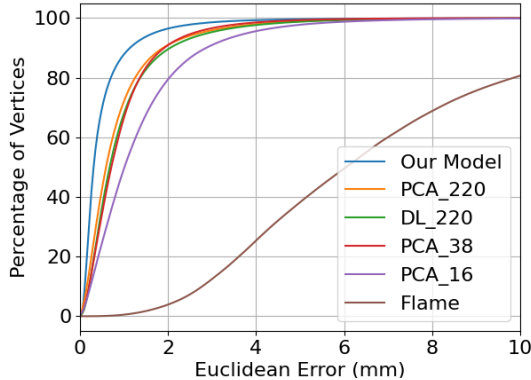


Figure 5. Cumulative per-vertex Euclidean error between PCA models, Flame, DL and our proposed model.

used the pre-trained model and the original code¹, which uses 8 components for identity and 8 for expressions.

Table 1 reports a quantitative comparison between our approach and the above mentioned methods. The significant improvement obtained by our method for all expressions comes out clearly from the table. On average, the improvement obtained with our approach is 40% better than the second best. In Figure 5 the cumulative per-vertex error distribution is reported to further highlight the precision of our approach, which can reconstruct almost 90% of the vertices with a < 1 mm error. Finally, in Figure 6 we show a qualitative example where we report error heatmaps in comparison with PCA.

4.4. Classification of Generated 4D Expressions

To evaluate the quality of the expression motions generated with Motion3DGAN, we implemented a classifier trained to recognize dynamic expressions. To this end, we

¹<https://github.com/soubhiksanyal/FLAME.PyTorch>

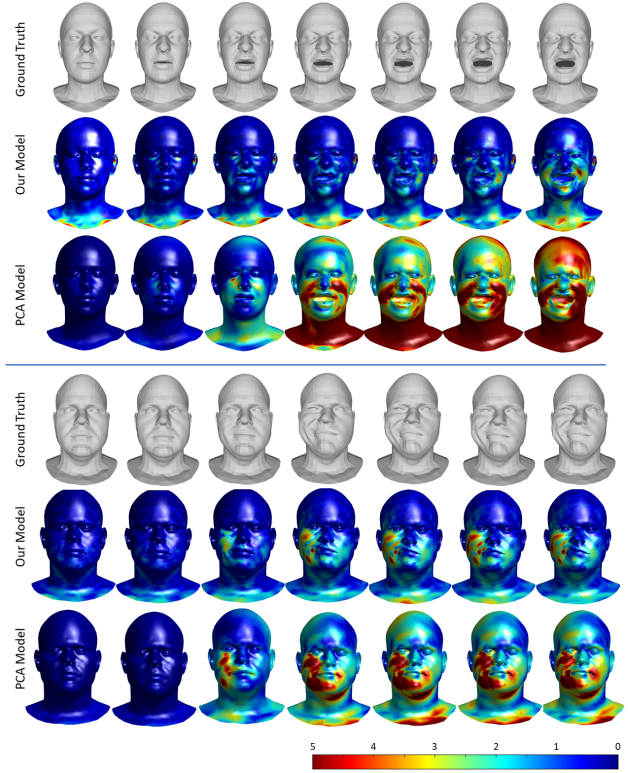


Figure 6. Color heatmap visualization of the error obtained with our model and PCA baseline against the ground truth meshes for two facial expression sequences.

used Motion3DGAN to generate 3D landmarks sequences, each of length 30, corresponding to the 12 expressions of the CoMA database. Then, we used them to generate 144 sequences of 30 meshes using our Expr-ED. To classify the resulting sequences, we trained a simple SVM classifier. We first projected each generated mesh of the sequence to a PCA space, resulting in a vector of 38 features each. The

Expression	PCA GT	PCA M-3DGAN	Ours GT	Ours M-3DGAN
Bareteeth	83.33	100.00	91.66	100.00
Cheeks-in	75.00	41.66	83.33	83.33
Eyebrow	91.66	83.33	100	100.00
High Smile	91.66	100.00	91.66	91.66
Lips Back	41.66	83.33	75.00	50.00
Lips up	100.00	0.00	100.00	91.66
Mouth down	75.00	16.66	83.33	33.33
Mouth Extreme	75.00	91.66	75.00	100.00
Mouth middle	33.33	33.33	50.00	16.66
Mouth Open	50.00	8.33	58.33	66.66
Mouth side	58.33	33.33	66.66	50.00
Mouth up	33.33	16.66	41.66	33.33
Total	67.36	50.69	76.38	66.66

Table 2. Classification accuracy in (%) of the data generated by the proposed method and PCA, when using ground truth (GT) landmarks and those generated by Motion3DGAN (M-3DGAN).

whole sequence is finally represented as concatenation of its corresponding mesh features. In Table 2, we report the classification accuracy obtained with mesh sequences generated with our Expr-ED, and the PCA baseline. In order to assess the quality of the Motion3DGAN generated sequences of landmarks, we also report the classification accuracy obtained using ground truth landmarks extracted from CoMA in place of Motion3DGAN landmarks.

In Table 2, the first aspect that can be noted is the effectiveness of Motion3DGAN in generating motions close to ground truth ones. This is evidenced by the high classification accuracy obtained for the majority of the classes, except *mouth_down* and *mouth_middle*, for which we obtained lower accuracy *w.r.t.* the sequences generated using ground truth landmarks. Table 2 also shows that the meshes generated with our Expr-ED are better recognized, and outperform those generated with PCA by 9%. This is consistent with our previous results, and demonstrates the high quality of the meshes obtained with our model. Furthermore, the performance deterioration obtained with PCA when using motion3DGAN landmarks is more important than that obtained with Expr-ED, which demonstrates the lower generalization capability of PCA *w.r.t.* our model.

4.5. Applications

Facial expression transfer from 2D to 3D. Here, we demonstrate how our proposed model can be exploited to transfer a facial expression from video sequences to a given 3D face. Given some video frames, we first detect the 3D facial landmarks in each frame using the detector proposed in [7]; then, we compute the SRVF of their motion using (2). Finally, the motion encoded in the SRVF is transferred to the neutral 3D landmarks of the given mesh using (3). In Figure 7, we show the results of transferring a facial expression from an image to a the CoMA 3D face template. We

observe that the 2D facial expressions, disgust, happiness and sadness, are correctly transferred to the 3D face. We highlight that these expressions are not included in CoMA, which demonstrates the high generalization capability of Expr-ED to generate 3D faces with novel expressions.

4D facial expression editing. Our model allows us to easily control the intensity of the generated/transferred expressions. Indeed, the motions generated by Motion3DGAN can be considered as controllable changes applied to the initial facial landmarks as expressed in (3). Consequently, we can amplify these changes by multiplying them by a factor ϵ to generate motions with different intensities, such that,

$$\alpha(t) = \epsilon \cdot \int_0^t \|q(s)\|q(s)ds + \alpha(0) . \quad (10)$$

In Figure 8, we show examples of generated expressions using the same SRVF motion applied to a neutral face with different intensities, controlled through the parameter ϵ ($\epsilon = 0.07$ and $\epsilon = 0.2$, respectively, for low and high intensity).

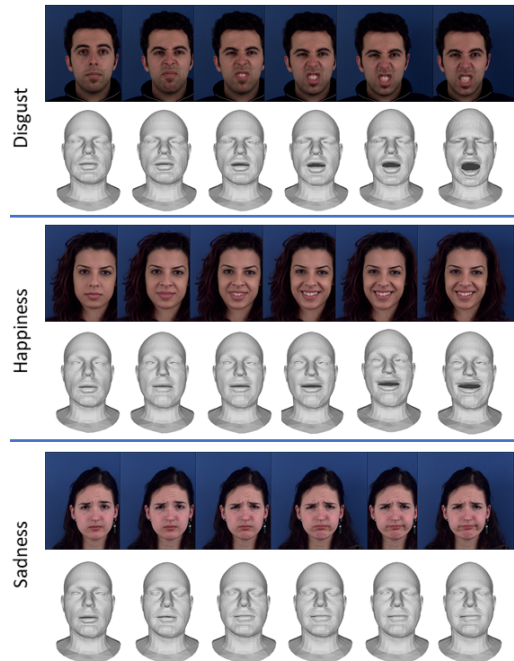


Figure 7. 3D Facial expression transfer. In each group, the expressions of the video frames in the top row taken from the MUG dataset [2] are transferred to the 3D faces in the bottom row.

5. Acknowledgments

This work was partially supported by the French State, managed by National Agency for Research (ANR) National Agency for Research (ANR) under the Investments for the future program with reference ANR-16-IDEX-0004 ULNE. This paper was also partially supported by European



Figure 8. 3D facial expression generation with controlled intensity. In each group, the same facial expression is illustrated with high and low intensities in the top and the bottom row, respectively.

Union’s Horizon 2020 research and innovation program under grant number 951911 - AI4Media. This work was also partially supported by the ANR project Human4D ANR-19-CE23-0020.

6. Conclusions

In this paper, we proposed a novel framework for dynamic 3D facial expression synthesis from still 3D neutral meshes. This is the first work that model the 3D facial motion using 3D facial landmarks. We proposed to disentangle the expression motion from the 3D mesh, by first generating the facial motion of 3D landmarks, then exploiting these landmarks to guide the deformation of 3D facial mesh. Through extensive experimentation, we showed the superiority of our model on the state-of-the-art, and demonstrated the high generalization capability of our Expr-ED model in generating strong and unseen expressions. We also show how our framework can be efficiently exploited for facial expression transfer from 2D to 3D and facial expression editing with controllable intensity.

7. Appendix

7.1. Landmarks Configuration

In Figure 9 we show, for three different expressions, the configuration of landmarks used to guide the generation of the facial expression.

7.2. 3D Expression Generation

Here we report few more qualitative examples. In Figure 10, we report a comparison between our Expr-ED, against PCA and FLAME [21]. Our method is capable

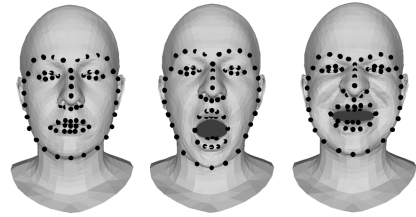


Figure 9. Landmarks configuration used to guide our model.

of correctly reproducing the expression associated to the 3D landmark configuration at different levels of intensity, while at the same time maintaining the structure of the input shape. On the other hand, PCA can correctly reproduce the expression at the cost of introducing a large amount of noise when the intensity of the expression increases. FLAME instead seems to fail in both the tasks.

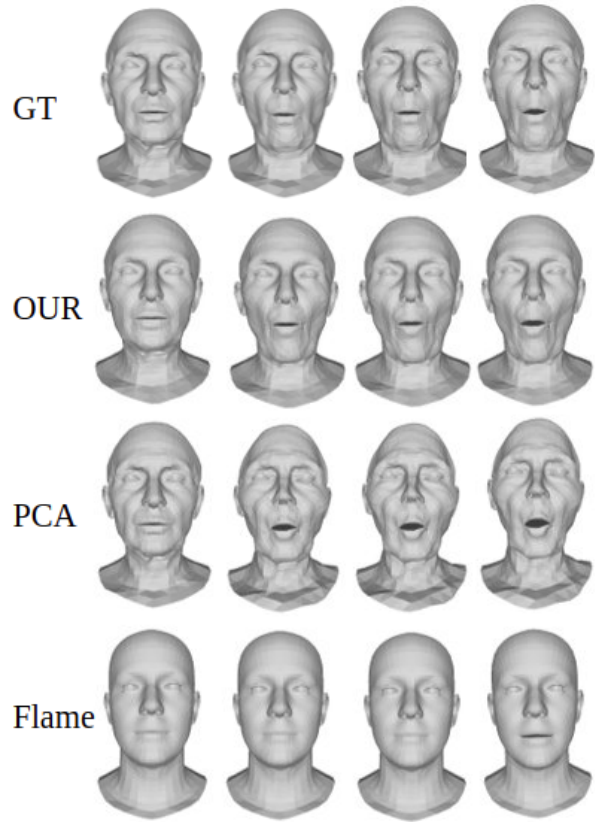


Figure 10. Qualitative example of 4D facial expression generation.

In Figure 11, we report additional examples for different expressions at the peak intensity. Our solution better captures the expression at a stronger intensity level with respect to PCA. Again, the reader can observe how the general shape is less affected by the deformation, ultimately resulting more realistic and faithful.

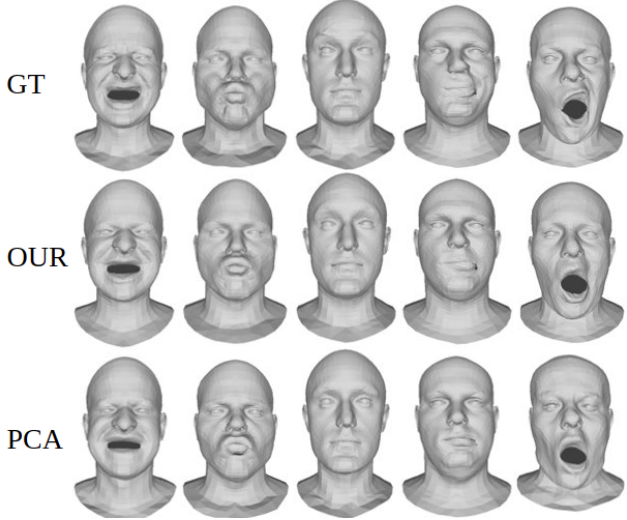


Figure 11. Qualitative example of 3D facial expression generation.

7.3. Motion3DGAN based 4D Sequences

In Figure 12, we instead report a qualitative comparison between frames of a mesh sequence obtained using the Motion3DGAN generated landmarks. In particular, we report an example of *high-smile* (Figure 12, top rows) and *mouth-extreme* (Figure 12, bottom rows) expressions. Note that Motion3DGAN is trained to replicate the expression given by the labels, and generates the landmark sequences from noise at test time. The goal is to replicate a particular expression, yet maintaining some degree of diversity from the ground-truth landmarks. Thus, the generated expressions might look a little different from those contained in the training data. However, from the reconstructed meshes in Figure 12, the reader can appreciate the quality of the generated sequences that correctly replicate the expression provided by the label. Similarly to Figure 11, the results with PCA look noisy and less natural with respect to those obtained with our solution.

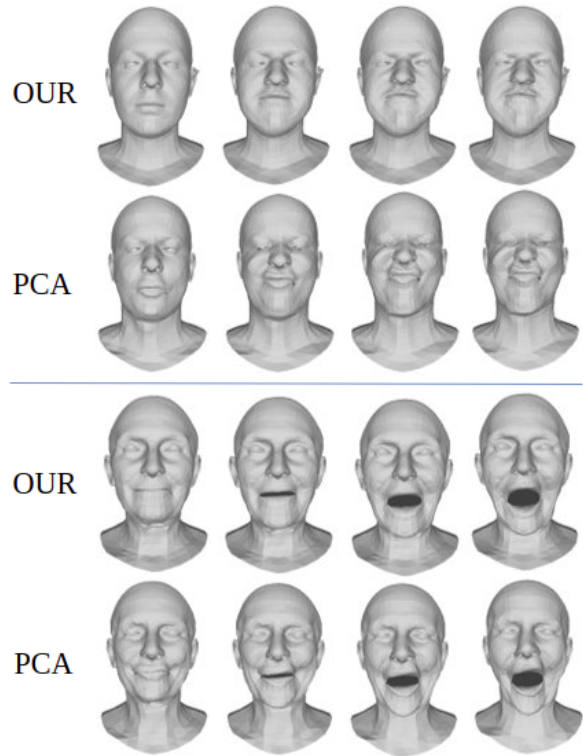


Figure 12. Meshes reconstructed from Motion3DGAN landmarks. Top rows: *high-smile*. Bottom rows: *mouth extreme*.

References

- [1] Victoria Fernandez Abrevaya, Stefanie Wuhrer, and Edmond Boyer. Multilinear autoencoder for 3d face model learning. In *IEEE Winter Conf. on Applications of Computer Vision (WACV)*, pages 1–9, 2018.
- [2] Niki Aifanti, Christos Papachristou, and Anastasios Delopoulos. The mug facial expression database. In *11th International Workshop on Image Analysis for Multimedia Interactive Services WIAMIS 10*, pages 1–4. IEEE, 2010.
- [3] Volker Blanz and Thomas Vetter. A morphable model for the synthesis of 3d faces. In *Annual Conf. on Computer Graphics and Interactive Techniques (SIGGRAPH)*, pages 187–194, 1999.
- [4] James Booth, Anastasios Roussos, Stefanos Zafeiriou, Allan Ponniah, and David Dunaway. A 3d morphable model learnt from 10,000 faces. In *IEEE Conf. on Computer Vision and Pattern Recognition (CVPR)*, pages 5543–5552, 2016.
- [5] Giorgos Bouritsas, Sergiy Bokhnyak, Stylianos Ploumpis, Stefanos Zafeiriou, and Michael Bronstein. Neural 3d morphable models: Spiral convolutional networks for 3d shape representation learning and generation. In *IEEE/CVF Int. Conf. on Computer Vision (ICCV)*, pages 7212–7221, 2019.
- [6] Michael M. Bronstein, Joan Bruna, Yann LeCun, Arthur Szlam, and Pierre Vandergheynst. Geometric deep learning: Going beyond euclidean data. *IEEE Signal Processing Mag.*, 34(4):18–42, 2017.
- [7] Adrian Bulat and Georgios Tzimiropoulos. How far are we from solving the 2d & 3d face alignment problem? (and a dataset of 230,000 3d facial landmarks). In *International Conference on Computer Vision*, 2017.
- [8] Chen Cao, Qiming Hou, and Kun Zhou. Displaced dynamic expression regression for real-time facial tracking and animation. *ACM Trans. on Graphics*, 33(4), July 2014.
- [9] Lisha Chen, Hui Su, and Qiang Ji. Deep structured prediction for facial landmark detection. In *Advances in Neural Information Processing Systems (Neurips)*, volume 32, 2019.
- [10] Daniel Cudeiro, Timo Bolkart, Cassidy Laidlaw, Anurag Ranjan, and Michael J. Black. Capture, learning, and synthesis of 3d speaking styles. In *IEEE/CVF Conf. on Computer Vision and Pattern Recognition (CVPR)*, pages 10093–10103, 2019.
- [11] Maxime Devanne, Hazem Wannous, Stefano Berretti, Pietro Pala, Mohamed Daoudi, and Alberto Del Bimbo. 3-D human action recognition by shape analysis of motion trajectories on Riemannian manifold. *IEEE Transactions on Cybernetics*, 45(7):1340–1352, 2014.
- [12] Xuanyi Dong, Yi Yang, Shih-En Wei, Xinshuo Weng, Yaser Sheikh, and Shou-I Yu. Supervision by registration and triangulation for landmark detection. *IEEE Trans. on Pattern Analysis and Machine Intelligence*, pages 1–1, 2020.
- [13] Hassen Drira, Boulbaba Ben Amor, Anuj Srivastava, Mohamed Daoudi, and Rim Slama. 3D face recognition under expressions, occlusions, and pose variations. *IEE Trans. on Pattern Analysis and Machine Intelligence*, 35(9):2270–2283, 2013.
- [14] Lijie Fan, Wenbing Huang, Chuang Gan, Junzhou Huang, and Boqing Gong. Controllable image-to-video translation: A case study on facial expression generation. In *Conf. on Artificial Intelligence (AAAI) Symposium on Educational Advances in Artificial Intelligence*, pages 3510–3517. AAAI Press, 2019.
- [15] Claudio Ferrari, Giuseppe Lisanti, Stefano Berretti, and Alberto Del Bimbo. A dictionary learning-based 3d morphable shape model. *IEEE Trans. on Multimedia*, 19(12):2666–2679, 2017.
- [16] Ishaan Gulrajani, Faruk Ahmed, Martin Arjovsky, Vincent Dumoulin, and Aaron C Courville. Improved training of wasserstein gans. In *Advances in Neural Information Processing Systems (NIPS)*, pages 5767–5777, 2017.
- [17] Rana Hanocka, Amir Hertz, Noa Fish, Raja Giryes, Shachar Fleishman, and Daniel Cohen-Or. Meshcnn: a network with an edge. *ACM Trans. Graph.*, 38(4):90:1–90:12, 2019.
- [18] Zhiwu Huang, Jiqing Wu, and Luc Van Gool. Manifold-valued image generation with wasserstein generative adversarial nets. In *The Thirty-Third AAAI Conference on Artificial Intelligence, AAAI 2019, The Thirty-First Innovative Applications of Artificial Intelligence Conference, IAAI 2019, The Ninth AAAI Symposium on Educational Advances in Artificial Intelligence, EAAI 2019, Honolulu, Hawaii, USA, January 27 - February 1, 2019*, pages 3886–3893. AAAI Press, 2019.
- [19] Anis Kacem, Mohamed Daoudi, Boulbaba Ben Amor, and Juan Carlos Alvarez-Paiva. A novel space-time representation on the positive semidefinite cone for facial expression recognition. In *Proceedings of the IEEE International Conference on Computer Vision*, pages 3180–3189, 2017.
- [20] Tero Karras, Timo Aila, Samuli Laine, Antti Herva, and Jaakko Lehtinen. Audio-driven facial animation by joint end-to-end learning of pose and emotion. *ACM Trans. on Graphics*, 36(4), July 2017.

[21] Tianye Li, Timo Bolkart, Michael Julian, Hao Li, and Javier Romero. Learning a model of facial shape and expression from 4D scans. *ACM Trans. on Graphics, (Proc. SIGGRAPH Asia)*, 36(6), 2017.

[22] Isaak Lim, Alexander Dielen, Marcel Campen, and Leif Kobbelt. A simple approach to intrinsic correspondence learning on unstructured 3d meshes. In *European Conf. on Computer Vision (ECCV) Workshops*, September 2018.

[23] Or Litany, Alex Bronstein, Michael Bronstein, and Ameesh Makadia. Deformable shape completion with graph convolutional autoencoders. In *IEEE/CVF Conf. on Computer Vision and Pattern Recognition*, pages 1886–1895, 2018.

[24] Rongye Meng, Sanping Zhou, Xingyu Wan, M. Li, and Jinjun Wang. Teacher-student asynchronous learning with multi-source consistency for facial landmark detection. *ArXiv*, abs/2012.06711, 2020.

[25] Stylianos Moschoglou, Stylianos Ploumpis, Michalis A. Nicolaou, Athanasios Papaioannou, and Stefanos Zafeiriou. 3dfacegan: Adversarial nets for 3d face representation, generation, and translation. *Int. Journal of Computer Vision*, 128:2534–2551, 2020.

[26] Naima Otberdout, Mohamed Daoudi, Anis Kacem, Lahoucine Ballihi, and Stefano Berretti. Dynamic facial expression generation on hilbert hypersphere with conditional Wasserstein generative adversarial nets. *IEEE Trans. on Pattern Analysis and Machine Intelligence*, pages 1–1, 2020.

[27] Pascal Paysan, Reinhard Knothe, Brian Amberg, Sami Romdhani, and Thomas Vetter. A 3d face model for pose and illumination invariant face recognition. In *IEEE Int. Conf. on Advanced Video and Signal Based Surveillance*, pages 296–301, 2009.

[28] Rolando Alexandros Potamias, Jiali Zheng, Stylianos Ploumpis, Giorgos Bouritsas, Evangelos Ververas, and Stefanos Zafeiriou. Learning to generate customized dynamic 3d facial expressions. In *European Conference on Computer Vision (ECCV)*, pages 278–294, 2020.

[29] Anurag Ranjan, Timo Bolkart, Soubhik Sanyal, and Michael J. Black. Generating 3D faces using convolutional mesh autoencoders. In *European Conference on Computer Vision (ECCV)*, pages 725–741, 2018.

[30] Anuj Srivastava, Eric Klassen, Shantanu H. Joshi, and Ian H. Jermyn. Shape analysis of elastic curves in euclidean spaces. *IEE Trans. on Pattern Analysis and Machine Intelligence*, 33(7):1415–1428, 2011.

[31] Nitika Verma, Edmond Boyer, and Jakob Verbeek. Feastnet: Feature-steered graph convolutions for 3d shape analysis. In *IEEE/CVF Conf. on Computer Vision and Pattern Recognition*, pages 2598–2606, 2018.

[32] Jun Wan, Zhihui Lai, Jing Li, Jie Zhou, and Can Gao. Robust facial landmark detection by multiorder multiconstraint deep networks. *IEEE Trans. on Neural Networks and Learning Systems*, pages 1–14, 2021.

[33] Wei Wang, Xavier Alameda-Pineda, Dan Xu, Pascal Fua, Elisa Ricci, and Nicu Sebe. Every smile is unique: Landmark-guided diverse smile generation. In *IEEE/CVF Conf. on Computer Vision and Pattern Recognition*, pages 7083–7092, 2018.

[34] Dan Zeng, Han Liu, Hui Lin, and Shiming Ge. Talking face generation with expression-tailored generative adversarial network. In *ACM Int. Conf. on Multimedia (MM’20)*, page 1716–1724, 2020.